Elastic scattering and vibrational excitation for electron impact on para-benzoquinone

D. B. Jones, F. Blanco, G. García, R. F. da Costa, F. Kossoski, M. T. do N. Varella, M. H. F. Bettega, M. A. P. Lima, R. D. White, and M. J. Brunger

Citation: The Journal of Chemical Physics **147**, 244304 (2017); doi: 10.1063/1.5010831
View online: https://doi.org/10.1063/1.5010831
View Table of Contents: http://aip.scitation.org/toc/jcp/147/24
Published by the American Institute of Physics

Elastic scattering and vibrational excitation for electron impact on *para*-benzoquinone

D. B. Jones,[1] F. Blanco,[2] G. García,[3] R. F. da Costa,[4,5] F. Kossoski,[4] M. T. do N. Varella,[6] M. H. F. Bettega,[7] M. A. P. Lima,[4] R. D. White,[8] and M. J. Brunger[1,a)]
[1]*College of Science and Engineering, Flinders University, GPO Box 2100, Adelaide, South Australia 5001, Australia*
[2]*Departamento de Física Atómica, Molecular y Nuclear, Universidad Complutense de Madrid, Madrid E-28040, Spain*
[3]*Instituto de Física Fundamental, CSIC, Serano 113-bis, E-28006 Madrid, Spain*
[4]*Instituto de Física "Gleb Wataghin," Universidade Estadual de Campinas, Campinas, São Paulo 13083-859, Brazil*
[5]*Centro de Ciências Exatas, Departamento de Física, Universidade Federal do Espírito Santo, 29075-901 Vitória, Espírito Santo, Brazil*
[6]*Instituto de Física, Universidade de São Paulo, Rua do Matão 1731, São Paulo 05508-090, Brazil*
[7]*Departamento de Física, Universidade Federal do Paraná, CP 19044, Curitiba, Paraná 81531-990, Brazil*
[8]*College of Science and Engineering, James Cook University, Townsville, Qld 4811, Australia*

(Received 27 October 2017; accepted 14 December 2017; published online 28 December 2017)

We report on theoretical elastic and experimental vibrational-excitation differential cross sections (DCSs) for electron scattering from *para*-benzoquinone ($C_6H_4O_2$), in the intermediate energy range 15–50 eV. The calculations were conducted with two different theoretical methodologies, the Schwinger multichannel method with pseudopotentials (SMCPP) and the independent atom method with screening corrected additivity rule (IAM-SCAR) that also now incorporates a further interference (I) term. The SMCPP with N energetically open electronic states (N_{open}) at the static-exchange-plus-polarisation (N_{open}ch-SEP) level was used to calculate the scattering amplitudes using a channel coupling scheme that ranges from 1ch-SE up to the 89ch-SEP level of approximation. We found that in going from the 38ch-SEP to the 89ch-SEP, at all energies considered here, the elastic DCSs did not change significantly in terms of both their shapes and magnitudes. This is a good indication that our SMCPP 89ch-SEP elastic DCSs are converged with respect to the multichannel coupling effect for the investigated intermediate energies. While agreement between our IAM-SCAR+I and SMCPP 89ch-SEP computations improves as the incident electron energy increases from 15 eV, overall the level of accord is only marginal. This is particularly true at middle scattering angles, suggesting that our SCAR and interference corrections are failing somewhat for this molecule below 50 eV. We also report experimental DCS results, using a crossed-beam apparatus, for excitation of some of the unresolved ("hybrid") vibrational quanta (bands I–III) of *para*-benzoquinone. Those data were derived from electron energy loss spectra that were measured over a scattered electron angular range of 10°–90° and put on an absolute scale using our elastic SMCPP 89ch-SEP DCS results. The energy resolution of our measurements was ~80 meV, which is why, at least in part, the observed vibrational features were only partially resolved. To the best of our knowledge, there are no other experimental or theoretical vibrational excitation results against which we might compare the present measurements. *Published by AIP Publishing.* https://doi.org/10.1063/1.5010831

I. INTRODUCTION

We have previously discussed why electron and photon studies on the quinone family, *para*-benzoquinone (pBQ, 1,4-benzoquinone, $C_6H_4O_2$, see Fig. 1) in particular, are important[1,2] and so we do not repeat that detail again here. Briefly, however, within the electron transport chain of photosynthesis and cellular respiration, quinones are a crucial molecular subunit as they are able to undergo reversible reduction. Hence they show potential as a sustainable, low-cost material for energy applications.[3] Quinone derivatives are also known to form in the combustion of fuels, and their presence has been observed in air particulate samples within urban environments.[4] Thus an understanding of the potential environmental implications of quinone and quinone-derivatives in our atmosphere, if they were to be employed large-scale in future technology developments, is also vital. pBQ, as the simplest quinone, has therefore served as a prototypical structure in an attempt to understand these and other complex chemical processes.

The spectroscopy of pBQ has been somewhat controversial due to it possessing many close-lying electronic-states. Good reviews on this aspect can be found in the work of Itoh[5] and more recently in the work of Ómarsson and Ingólfsson.[6] There have also been photoelectron,[7–10] Penning ionisation,[11]

a)Author to whom correspondence should be addressed: Michael.Brunger@flinders.edu.au

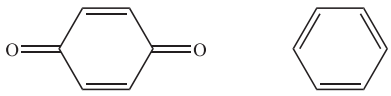

para-benzoquinone (pBQ) benzene

FIG. 1. Schematic representation of the *para*-benzoquinone (pBQ, $C_6H_4O_2$) and benzene (C_6H_6) structures.

and matrix isolation[12] studies in order to provide insights into the cationic structure of pBQ. The gas-phase photoabsorption spectrum in the visible[13–15] and UV[2,16–18] spectral regions has been extensively studied, while in the vacuum ultraviolet (VUV) range, we note the low resolution study of Brint *et al.*[19] and our own high resolution investigation.[2] From the electron scattering viewpoint, most work has been undertaken on electron attachment and resonances.[20–22] In addition, Allan[23,24] has also performed transmission electron impact energy loss spectra measurements to gain insights into attachment and excitation processes. Further, the dynamics of electron impact ionisation of pBQ have been investigated.[1] More recently, Jones *et al.*[2] studied the electronic-state spectroscopy of pBQ using photoabsorption and electron energy loss spectroscopy (EELS). That latter work was supported by detailed quantum chemical calculations.[2] The latest investigation, by Loupas and Gorfinkiel,[25] employed the R-matrix formalism to study low-energy resonances in the elastic and electronically inelastic scattering channels of pBQ. Significant electron capture behaviour, leading to resonance structures in the integral cross section (ICS), was found by those authors.[25]

Over the last decade or so, we have devoted quite a lot of effort, both theoretical and experimental, to study electron scattering phenomena from biomolecules such as water (e.g., Refs. 26 and 27), tetrahydrofuran (e.g., Refs. 28–30), pyrimidine (e.g., Refs. 31–36), and α-tetrahydrofurfuryl alcohol (e.g., Refs. 37–40) and technologically important molecules such as phenol (e.g., Refs. 41–46) and furfural (e.g., Refs. 47–52). Some of those species studied have been recently reviewed by Brunger[53] and Gorfinkiel and Ptasinska.[54] Aside from investigating things like the effect of the molecular electronic properties (i.e., the dipole moment and dipole polarisability) on the collision behaviour and benchmarking our theoretical and experimental results against each other where possible, we have also attempted to contribute cross sections to databases (e.g., LXCaT[55]) that might then be employed with Monte Carlo techniques to simulate charged-particle track behaviour in matter.[56–59] Additionally, such databases might also be used in conjunction with Monte Carlo on Boltzmann equation approaches to simulate the transport behaviour of electrons under the influence of an applied electric field on those molecules.[60–65] In the latter case, our simulation results are often benchmarked against independent electron swarm experiments that measure transport coefficients such as the drift velocity and Townsend ionisation and diffusion coefficients.[63] In this context, the present investigation on elastic scattering and vibrational excitation seeks to contribute towards building a "correct, absolute, and comprehensive"[66] database, in order to similarly undertake charged-particle track Monte Carlo simulations and Boltzmann equation solution analyses for electron transport in pBQ.

The outline of the remainder of this paper is as follows. In Sec. II, we briefly describe the details of our theoretical calculations and experimental procedures, with our results being presented and discussed in Sec. III. Finally, in Sec. IV, some conclusions from our investigation are summarised.

II. THEORETICAL AND EXPERIMENTAL METHODS

A. Schwinger multichannel method with pseudopotentials (SMCPP)

The Schwinger multichannel (SMC) method[67] for electron–molecule scattering is a variational approach especially designed to deal with targets of arbitrary geometries. To accomplish this, it uses square integrable basis functions in order to obtain the scattering amplitudes. The method takes into account important effects such as the electron exchange, the electron–target polarisation interaction, and the possibility of flux competition between the elastic and inelastic channels through electronic multichannel coupling. The significant computational cost for getting meaningful results for polyatomic targets like pBQ led us to use parallel computing[68] in an implementation that also employs norm-conserving pseudopotentials[69] (SMCPP) and single-excitation configuration interaction techniques for the target description.[70] Since our method has been recently reviewed,[71] here we only need to give the working expression for the scattering amplitude as

$$f\left(\mathbf{k}_f, \mathbf{k}_i\right) = -\frac{1}{2\pi} \sum_{m,n} \left\langle S_{\mathbf{k}_f} | V | \chi_m \right\rangle (d^{-1})_{mn} \left\langle \chi_n | V | S_{\mathbf{k}_i} \right\rangle , \qquad (1)$$

where

$$d_{mn} = \left\langle \chi_m \left| \left[\frac{\hat{H}}{N+1} - \frac{\hat{H}P + P\hat{H}}{2} + \frac{PV + VP}{2} - VG_P^{(+)}V \right] \right| \chi_n \right\rangle . \qquad (2)$$

In the expression above, P is a projector onto N_{open} energy-allowed target electronic channels, i.e.,

$$P = \sum_{\ell=1}^{N_{\text{open}}} |\Phi_\ell\rangle \langle \Phi_\ell| , \qquad (3)$$

with $|\Phi_\ell\rangle$ written as a single-excitation configuration-interaction wave function, $G_P^{(+)}$ is the free-particle Green's function projected onto P space, V is the electron–target interaction potential, $\mathbf{k}_i(\mathbf{k}_f)$ is the incoming (outgoing) projectile wave vector, and $\hat{H} = E - H$ is the total energy (ground state energy plus the kinetic energy of the incoming electron) minus the Hamiltonian of the $(N + 1)$ electrons under the field of the fixed nuclei. The latter is given by $H = H_0 + V$, where H_0 describes the non-interacting electron–molecule system and $S_{\mathbf{k}}$ is a solution of H_0. Namely, it is the product of a plane wave (projectile) and a target state $|\Phi_\ell\rangle$. For the expansion of the variational scattering wave function, the method employs trial basis sets comprising $(N + 1)$-particle configuration state functions (CSFs), denoted by $|\chi_m\rangle$, that are built from spin-adapted, anti-symmetrised products of target electronic states and projectile scattering orbitals. The energetically open electronic collision channels are included in the P space, and the dynamical response of the target electrons to the projectile field (correlation-polarisation effects) is accounted for through virtual excitations of the target. Here, the CSFs are given by

$$|\chi_m\rangle = A_{N+1}\,|\Phi_i(1,\ldots,N)\rangle \otimes \left|\phi_j(N+1)\right\rangle, \qquad (4)$$

where for $i > 0$, $|\Phi_i\rangle \equiv^{(2S+1)}(h_i \rightarrow p_i)$ is a singly excited state obtained by promoting one electron to create a hole in the orbital (h_i) of the ground state $|\Phi_0(1,\ldots,N)\rangle$ and occupying a particle orbital (p_i), with either singlet ($S = 0$) or triplet ($S = 1$) spin coupling, although in practice only ($N + 1$)-electron configurations with total spin $S = 1/2$ (doublets) are taken into account. If we have N_{open} states in Eq. (3), this level of calculation is called an N_{open}-channel coupling scheme at the static-exchange-plus polarisation (N_{open}ch-SEP) approximation. N_{open}ch-SE denotes calculations performed at the static-exchange level of approximation with N_{open} states. In the present implementation, elastic scattering at discrete intermediate energies (15–50 eV) is considered with the number of open scattering channels (N_{open}) ranging from 1 to 89 channels in our computations. Furthermore, in this energy range, we did not detect any major differences in the elastic differential cross section (DCS) results between our SEP and SE calculations. As a consequence, in this paper, we simply report our SMCPP-SEP elastic DCS data (see Table I).

In order to transform the scattering amplitude from the body-fixed frame (the reference frame best suited for carrying out the calculations) to the laboratory-fixed frame (the reference frame where the z-axis is aligned with the direction of the incident wave vector, i.e., $\mathbf{k}_i = k_i\hat{\mathbf{z}}$), we expand $\mathbf{k}_f$ in terms of partial waves,[72]

$$f(\mathbf{k}_f,\mathbf{k}_i) \equiv \left\langle \mathbf{k}_f|f|\mathbf{k}_i\right\rangle = \sum_{\ell=0}^{\ell_{\max}}\sum_{m=-\ell}^{\ell}\left\langle \mathbf{k}_f|\ell m\right\rangle f(\ell m,\mathbf{k}_i), \qquad (5)$$

where $\left\langle \mathbf{k}_f|\ell m\right\rangle$ is a spherical harmonic that can be easily converted from the body- to the laboratory-frame and

TABLE I. Differential cross sections ($\times 10^{-16}$ cm^2/sr) for elastic scattering of electrons from pBQ calculated within the SMCPP framework utilizing an 89-open channel (ground state plus 44 singlet states and 44 triplet states) coupling scheme at selected impact energies (16–50 eV) and angles (0°–180°). Results shown are for the SEP level of approximation.

Angle (deg)	σ_{Elas} (E_0 = 16 eV)	σ_{Elas} (E_0 = 20 eV)	σ_{Elas} (E_0 = 25 eV)	σ_{Elas} (E_0 = 30 eV)	σ_{Elas} (E_0 = 35 eV)	σ_{Elas} (E_0 = 40 eV)	σ_{Elas} (E_0 = 45 eV)	σ_{Elas} (E_0 = 50 eV)
0	82.0	86.7	91.4	90.0	88.3	88.2	87.0	84.5
5	75.3	78.9	82.1	80.0	77.9	77.1	75.5	72.8
10	58.3	59.1	59.3	56.0	53.1	51.3	48.9	46.2
15	37.8	36.3	34.0	30.5	27.6	25.4	23.1	20.9
20	20.5	18.2	15.5	12.8	10.9	9.40	7.96	6.73
25	9.42	7.59	5.75	4.45	3.70	3.11	2.57	2.18
30	3.89	2.95	2.18	1.80	1.71	1.62	1.52	1.49
35	1.75	1.42	1.25	1.19	1.26	1.29	1.30	1.32
40	1.08	1.00	1.01	0.99	1.05	1.11	1.13	1.13
45	0.89	0.87	0.92	0.91	0.96	1.01	1.03	1.02
50	0.83	0.81	0.90	0.89	0.92	0.93	0.93	0.92
55	0.80	0.78	0.90	0.88	0.87	0.86	0.85	0.83
60	0.76	0.75	0.87	0.84	0.83	0.81	0.80	0.76
65	0.71	0.72	0.82	0.79	0.79	0.77	0.74	0.68
70	0.68	0.70	0.75	0.73	0.74	0.70	0.66	0.62
75	0.66	0.69	0.70	0.68	0.69	0.64	0.60	0.60
80	0.65	0.68	0.67	0.67	0.66	0.60	0.58	0.60
85	0.63	0.66	0.67	0.67	0.65	0.59	0.57	0.58
90	0.61	0.65	0.69	0.68	0.65	0.61	0.59	0.61
95	0.60	0.65	0.71	0.69	0.67	0.65	0.65	0.67
100	0.61	0.67	0.73	0.72	0.72	0.71	0.72	0.74
105	0.64	0.71	0.76	0.76	0.78	0.78	0.78	0.77
110	0.70	0.76	0.81	0.82	0.84	0.83	0.81	0.77
115	0.76	0.84	0.87	0.87	0.88	0.87	0.82	0.77
120	0.83	0.93	0.94	0.92	0.92	0.90	0.85	0.79
125	0.90	1.02	1.01	0.98	1.00	0.99	0.94	0.86
130	0.95	1.08	1.07	1.07	1.11	1.13	1.07	0.99
135	1.00	1.13	1.13	1.16	1.23	1.26	1.20	1.13
140	1.04	1.15	1.19	1.26	1.33	1.37	1.30	1.24
145	1.11	1.19	1.29	1.39	1.43	1.44	1.38	1.33
150	1.22	1.27	1.46	1.55	1.55	1.52	1.47	1.43
155	1.33	1.39	1.70	1.75	1.70	1.63	1.59	1.54
160	1.42	1.50	1.95	1.95	1.84	1.77	1.74	1.67
165	1.43	1.56	2.15	2.07	1.93	1.87	1.88	1.79
170	1.37	1.55	2.25	2.09	1.94	1.92	1.97	1.86
175	1.29	1.50	2.28	2.05	1.90	1.91	2.01	1.89
180	1.25	1.48	2.27	2.02	1.88	1.90	2.02	1.89

$f(\ell m, \mathbf{k}_i) = \langle \ell m | f | \mathbf{k}_i \rangle$ can be interpreted as the scattering amplitude of an electron entering the interaction region in a plane-wave $|\mathbf{k}_i\rangle$ and leaving it in a partial wave $|\ell m\rangle$. For completeness, we also note that we average the cross sections over $d^2\mathbf{k}_i$ in the body-frame, which is equivalent to averaging over the molecular orientations in the laboratory-frame. In the present study, and consistent with what we found in our earlier work in furfural,[48] we found convergence was achieved with $\ell_{\max} = 13$.

B. Independent atom model with screening corrected additivity rule and interference terms (IAM-SCAR+I)

The IAM-SCAR+I method has been previously described,[73,74] most recently by Traoré Dubuis *et al.*,[52] so that only a brief précis is presented here. The fundamental premise of this independent atom model approach is that the molecular target of interest is not considered as a single multi-centre target, but as an aggregate of individual atoms.[75] As a result, this approximation effectively assumes that the molecular binding does not affect the electronic distribution of the atom so that each atom scatters independently from the others. Put simply, the atoms of the molecule are viewed as isolated entities. Hence the initial task in any IAM-SCAR+I computation is to describe the electron scattering from the atoms constituting the molecular target (here carbon, hydrogen, and oxygen). The electron–atom interaction is represented by an *ab initio* complex optical potential, where the real part accounts for elastic scattering while the imaginary part represents the inelastic processes. Note that these inelastic processes are considered as "absorption" channels from the incident electron beam. The complex potential for each atom in the molecule is represented by

$$\begin{aligned} V_{\text{opt}}(\mathbf{r}) &= V_{\text{R}}(\mathbf{r}) + iV_{\text{abs}}(\mathbf{r}) \\ &= V_{\text{s}}(\mathbf{r}) + V_{\text{ex}}(\mathbf{r}) + V_{\text{pol}}(\mathbf{r}) + iV_{\text{abs}}(\mathbf{r}). \end{aligned} \tag{6}$$

In Eq. (6), the real part (R) consists of three terms: (i) a static term (V_{s}) derived from a Hartree-Fock calculation of the atomic charge distributions,[76] (ii) an exchange term (V_{ex}) which accounts for the indistinguishability of the incident and target electrons,[77] and (iii) a polarisation potential (V_{pol}) that describes the long-range interactions.[78] Finally, the imaginary part of the potential defined by the absorption potential (V_{abs}) is based on a quasi-free model developed by Staszewska *et al.*[79] Initially, quite significant discrepancies between the experimental data and the optical potential model were found although these were subsequently corrected.[80,81] With those changes, the Madrid team has developed a method capable of representing electron-atom scattering over a broad range of energies and targets (e.g., Ref. 82).

The electron–molecule cross sections are now computed from the atomic data by the additivity rule (AR).[83] Within that approach, the molecular scattering amplitude is determined from the sum of all the relevant atomic amplitudes, including the phase coefficients, from which the molecular DCSs can be generated. Although not strictly relevant to this paper, for completeness, we note that integral cross sections (ICSs) can then be derived by integrating those DCS. The total cross sections (TCSs) are determined from the sum of the elastic ICS and the absorption ICS (for all inelastic processes except rotations and vibrations). The principal limitation of this approach is that no molecular structure is considered, making it valid only for fast incident electrons (typically $\geqslant$100 eV[81] although the precise energy is a little species dependent) which effectively "see" the target molecule as a sum of individual atoms. For lower incident energies, the atomic cross sections are sufficiently large to overlap with one another, leading to an overestimation of the AR molecular cross sections. To solve that limitation, at least in part, Blanco and García[84] developed a screening corrected additivity rule (SCAR) procedure which takes into account the geometric features of the molecule by introducing some screening coefficients. More recently, they have also incorporated some interference (I) term corrections to the SCAR method.[74] Within those SCAR and SCAR+I approaches, the range of validity of the model might be extended down to incident electron energies of 20–30 eV. Certainly there is some evidence to suggest that both the IAM-SCAR or IAM-SCAR+I methods are quite powerful tools for calculating cross sections at intermediate to high energies (i.e., ~50–10 000 eV).[59,85–87]

C. Experimental details

A typical EELS for electron–pBQ scattering, measured as a part of this study, is given in Fig. 2. Those data were acquired with a crossed-beam apparatus housed at Flinders University,[88] which has been documented in detail before. Briefly, however, a monochromated beam of electrons with energies (E_0) of 20 eV, 30 eV, or 40 eV, and a typical flux producing a current in the range 0.8–3 nA in a Faraday cup, was incident on an orthogonal beam of pBQ. *Para*-benzoquinone was a rather difficult target to work with, with details of our processes for obtaining a stable beam now being given. The pBQ vapour was obtained through sublimation of its crystalline solid (Sigma-Aldrich, >98% assay). Here the solid sample was heated

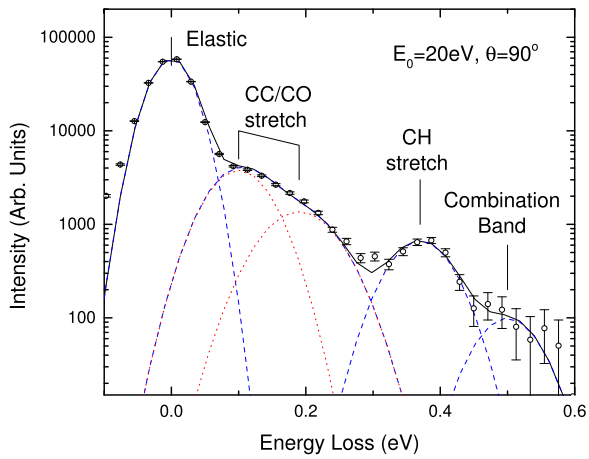

FIG. 2. An example electron energy loss spectrum for pBQ obtained at an incident electron energy of 20 eV and a 90° scattering angle. Also shown is our fitting to this spectrum, showing peaks for the elastic feature, and bands for excitation to unresolved bands describing composite vibrational modes. Here the assignment of features within each band is summarised in Table II. The overall spectral deconvolution plot is denoted by the solid black line, while the fits to the various composite vibrational features (bands I–III) and the elastic peak are also shown by the dashed blue line. Here the dotted red lines denote fits for the individual Gaussian functions, which are combined into a single composite vibrational feature.

to 55 °C. The vapour was transported through a gas handling system, heated to 70 °C to minimise recrystallisation in the gas lines, where it was introduced into the chamber (also heated to 70 °C) through a variable leak valve coupled to a single channel capillary (0.7 mm inner diameter) molybdenum needle that was used as the beam forming device. Note that the sample reservoir, gas handling lines, leak valve, and scattering chamber were all insulated from their surrounds to keep their temperature as stable as possible. Under the stable beam conditions maintained during the EELS measurements, the pBQ pressure in the vacuum chamber never exceeded 5×10^{-6} Torr but was typically ~2–3 $\times 10^{-6}$ Torr, in order to minimise any possible multiple scattering effects. Finally, the recent study on decomposition of biomolecules, specifically uracil and a range of uracil derivatives related to positron emission tomography (PET) studies,[89] indicated that they are stable against thermal decomposition up to ~200 °C. As this temperature is much higher than those we employed in this investigation, we are confident that pBQ does not decompose here.

The intersection of the electron and pBQ beams defines a collision volume (interaction region), and those electrons which collided with the molecules and scattered at some angle θ, called the electron scattering angle, were energy analysed using a hemispherical selector before being detected with a channel electron multiplier. Note that the angular range of the present EELS was 10°–90°, while the angular resolution of the analyser is 2°. Further note that the overall instrumental energy resolution employed in our measurements was ~80 meV (FWHM), which was insufficient to resolve many of the vibrational modes from one another (see Table II). Consequently, composite vibrational mode cross sections for bands I, II, and III are reported here (see Fig. 2). As noted previously, pBQ was a particularly challenging target to work with owing to the low count rates observed under the conditions to maintain a stable beam for our system. These conditions were necessary to overcome issues with pBQ vapour recrystallising within the gas handling system and causing pressure drops/pressure spikes. As such, the accumulation time for the energy loss spectra, recorded using a multichannel scaler (MCS) synchronised to a linear voltage ramp that varied the detected energy loss over the required range, at specific impact energies and scattering angles, ranged from 1 day to 3 weeks of continuous run-time. Here we note that this work encompasses a broader range of energy loss values covering electronic excitation, with the results from that work to be reported elsewhere.

TABLE II. The pBQ composite vibrational feature peak positions, widths (FWHM), and assignments. Here the uncertainty in the peak position and widths represents the standard deviation of the fitting parameter employed to obtain the best fit to the measured spectra across all incident electron energies and scattering angles.

Band	Position (eV)	Width (eV)	Vibrational modes	Assignment
Elastic	0.00	0.08 ± 0.01	ν_{23}–ν_{30}	Ring distortions
Band I	0.11 ± 0.02	0.10 ± 0.02	ν_5–ν_{23}	CC-stretching/CH bending/
	0.21 ± 0.03	0.11 ± 0.02		CO stretching
Band II	0.37 ± 0.02	0.11 ± 0.02	ν_1–ν_4	CH stretching
Band III	0.53 ± 0.02	0.11 ± 0.02		Combination band

Depending on the experimental conditions, energy loss spectra at specific incident energies and scattered electron angles were run multiple times or collected in a piecewise fashion over the extended collection period required to obtain reasonable counting statistics required to deconvolute the spectra (as detailed below). In this way, we were able to check that the ratio of inelastic to elastic features was consistent to be within experimental uncertainty across the multiple experimental runs or partial runs in situations where an extended accumulation period was required.

The ground and excited state vibrational energies have been extensively studied by Weber *et al.*,[90] where they have reviewed the available experimental values. We have therefore assigned specific normal modes to our composite vibrational features, with these assignments being contained in Table II. Further, the present vibrational state assignments are consistent with those we obtained in our own optimisation and frequency calculations using DFT in GAUSSIAN at the B3LYP level with an aug-cc-PVDZ basis set.[91]

The EELS were deconvoluted into contributions arising from each individual or unresolved combination of excited vibrational states.[92] In each case, one or two Gaussian functions were used to describe the spectral profile for each resolvable inelastic feature and the elastic peak (see Table II), with a typical example of the result from those fits being given in Fig. 2. Here the amplitudes of the Gaussian functions (in which the peak energies and peak widths are fixed in each case) were then varied in a least-squares fitting procedure[92] to provide the best fit to the measured spectra. The ratio (R) of the area under the fitting function for each ith vibrational feature to that under the elastic peak, at each E_0 and θ, is quite simply related to the ratio of the DCSs (σ) from

$$R_i(E_0, \theta) = \frac{\sigma_i(E_0, \theta)}{\sigma_0(E_0, \theta)}. \quad (7)$$

Note that Eq. (7) is only valid if the transmission efficiency of the analyser remains constant over the E_L and angular range studied or is at least well characterised.[66,88] Following a technique similar to that of Allan,[93] an additional focussing lens (synchronised to the voltage ramp) was also employed to minimise variations in the analyser transmission efficiency for electrons detected with different values of E_L. Of course, in the present experiments, the scattered electron energies are all very similar to those for E_0 so that a significant transmission effect is not expected here. Nonetheless, we place a very conservative uncertainty of 20% on our analyser efficiency being unity.[66] The present measured R_i for the composite vibrational mode bands I, II, and III are summarised in Tables III–V, respectively.

It is immediately apparent from Eq. (7) that the product $R_i \times \sigma_0$ gives the required composite vibrational mode DCSs provided the elastic DCSs (σ_0) are known. Those results for bands I, II, and III can also be found in Tables III–V. In this study, we have used the previously discussed SMCPP results for 89 open channels and at the SEP level of approximation (see Table I) to undertake that normalisation. Note that no measured elastic DCSs for electron scattering from pBQ are currently published, and given the challenges we found in using pBQ, we are skeptical that any applications of the relative flow

TABLE III. Differential cross sections ($\times 10^{-16}$ cm^2/sr) for vibrational excitation of the composite CC and CO stretching and CH bending modes (vibrational band I, $E_L \sim 0.11$–0.21 eV) of pBQ.

	$E_0 = 20$ eV			$E_0 = 30$ eV			$E_0 = 40$ eV		
Angle (deg)	Ratio	DCS	Uncertainty (%)	Ratio	DCS	Uncertainty (%)	Ratio	DCS	Uncertainty (%)
10	0.022	1.330	75	0.011	0.620	84	0.045	2.297	95
20	0.018	0.326	66	0.021	0.266	91	0.016	0.153	73
30	0.062	0.184	59	0.039	0.071	67	0.033	0.053	64
40	0.375	0.376	74	0.226	0.224	52	0.178	0.197	40
50	0.118	0.096	71	0.055	0.050	80	0.034	0.032	23
60	0.083	0.062	72	0.060	0.051	84	0.038	0.031	25
70	0.129	0.090	77	0.078	0.057	75	0.057	0.040	24
80	...	...	...	0.100	0.066	80	0.077	0.046	23
90	0.133	0.087	74	0.114	0.078	80	0.082	0.050	24

technique[94] to attempt such measurements are likely. This follows as in using the relative flow method, one necessarily cycles the target and standard gases throughout the measurements.[94] In our experience, the pBQ pressure took some time to stabilise, making the duty cycle in a relative flow measurement with it as the target species highly problematic. The efficacy of using our SMCPP 89ch-SEP results, to effect the normalisation of our R_i via Eq. (7), is discussed later in Sec. III. Here we simply note that similar to what we found in our investigations in phenol[42] and furfural,[48] we believe the current elastic SMCPP results are a valid choice.

The current composite vibrational excitation DCSs for bands I, II, and III in pBQ are given in Tables III–V, respectively. Error estimates on those data are also provided in each of these tables. Particular attention to the identification and

TABLE IV. Differential cross sections ($\times 10^{-16}$ cm^2/sr) for vibrational excitation of the composite CH stretching modes and CC/CO overtones (vibrational band II, $E_L \sim 0.37$ eV) of pBQ.

	$E_0 = 20$ eV			$E_0 = 30$ eV			$E_0 = 40$ eV		
Angle (deg)	Ratio	DCS	Uncertainty (%)	Ratio	DCS	Uncertainty (%)	Ratio	DCS	Uncertainty (%)
10	1.35×10^{-3}	7.96×10^{-2}	74	2.77×10^{-4}	1.55×10^{-2}	48	2.58×10^{-4}	1.32×10^{-2}	74
20	5.56×10^{-4}	1.01×10^{-2}	39	4.33×10^{-4}	5.55×10^{-3}	95	4.94×10^{-4}	4.64×10^{-3}	59
30	8.17×10^{-3}	2.41×10^{-2}	24	3.40×10^{-3}	6.14×10^{-3}	95	2.58×10^{-3}	4.18×10^{-3}	55
40	5.02×10^{-2}	5.03×10^{-2}	23	4.79×10^{-2}	4.75×10^{-2}	25	5.70×10^{-2}	6.33×10^{-2}	53
50	1.38×10^{-2}	1.12×10^{-2}	28	4.08×10^{-3}	3.65×10^{-3}	45	2.97×10^{-3}	2.78×10^{-3}	36
60	7.37×10^{-3}	5.49×10^{-3}	23	3.23×10^{-3}	2.72×10^{-3}	55	4.51×10^{-3}	3.66×10^{-3}	39
70	1.13×10^{-2}	7.92×10^{-3}	27	3.41×10^{-3}	2.48×10^{-3}	45	5.09×10^{-3}	3.58×10^{-3}	39
80	...	...	...	4.88×10^{-3}	3.25×10^{-3}	30	6.13×10^{-3}	3.68×10^{-3}	45
90	1.65×10^{-2}	1.07×10^{-2}	22	6.43×10^{-3}	4.38×10^{-3}	58	4.04×10^{-3}	2.47×10^{-3}	95

TABLE V. Differential cross sections ($\times 10^{-16}$ cm^2/sr) for vibrational excitation of combination CH stretching modes (vibrational band III, $E_L \sim 0.53$ eV) of pBQ.

	$E_0 = 20$ eV			$E_0 = 30$ eV			$E_0 = 40$ eV		
Angle (deg)	Ratio	DCS	Uncertainty (%)	Ratio	DCS	Uncertainty (%)	Ratio	DCS	Uncertainty (%)
10	1.84×10^{-4}	1.09×10^{-2}	95	4.08×10^{-5}	2.28×10^{-3}	95	1.26×10^{-4}	6.45×10^{-3}	76
20	2.47×10^{-5}	4.50×10^{-4}	74	9.77×10^{-5}	1.25×10^{-3}	95	3.19×10^{-7}	2.99×10^{-6}	83
30	1.56×10^{-3}	4.59×10^{-3}	44	5.71×10^{-4}	1.03×10^{-3}	95	2.29×10^{-4}	3.71×10^{-4}	95
40	6.95×10^{-3}	6.97×10^{-3}	31	6.37×10^{-3}	6.32×10^{-3}	85	5.47×10^{-3}	6.08×10^{-3}	60
50	2.03×10^{-4}	1.65×10^{-4}	95	1.02×10^{-5}	9.15×10^{-6}	95	6.04×10^{-4}	5.65×10^{-4}	95
60	8.61×10^{-4}	6.41×10^{-4}	44	7.07×10^{-4}	5.95×10^{-4}	95	4.18×10^{-4}	3.39×10^{-4}	82
70	1.33×10^{-3}	9.33×10^{-4}	95	1.16×10^{-4}	8.41×10^{-5}	95	3.48×10^{-4}	2.45×10^{-4}	83
80	...	...	...	5.00×10^{-4}	3.33×10^{-4}	95	1.32×10^{-4}	7.92×10^{-5}	95
90	2.44×10^{-3}	1.59×10^{-3}	25	6.25×10^{-4}	4.25×10^{-4}	95	1.02×10^{-3}	6.21×10^{-4}	95

quantification of all possible sources of error has been made in this investigation. Here the statistical errors associated with the scattering intensity measurements for the elastic peak and bands I and II are usually small although for the weaker band III feature they can become important. As noted above, an additional error due to our analyser transmission calibration (~20%) must also be considered. While the inherent error in our SMCPP elastic DCS computations is negligible, we have found from the past experience[42,71] that it can often reproduce the experimental data to 10% or better at energies between 20 and 40 eV. Hence, a 10% uncertainty on our elastic DCS has been incorporated into our analysis. Another important source of possible errors is that associated with the numerical deconvolution of the energy loss spectra, so an allowance for this is also made in the overall composite vibrational DCS uncertainties. When all these factors are combined in quadrature, the errors in the composite vibrational mode DCS (see Tables III–V) are usually found to be in the range 22%–95%. Note that the largest uncertainties often occur due to the poorer statistics associated with the weaker band III feature or at the more forward scattering angles where the elastic scattering intensity is much greater than that for vibrational excitation. This can make it particularly challenging to uniquely deconvolute these features.

III. RESULTS AND DISCUSSION

In Figs. 3 and 4, we demonstrate how the inclusion of multichannel coupling impacts on our calculated elastic differential cross sections. We do this specifically in Fig. 3 for the incident electron energies 15 or 16 eV, 20 eV, 25 eV, and 30 eV, while in Fig. 4, we present our elastic DCS results for the incident electron energies 35 eV, 40 eV, 45 eV, and 50 eV. Note that in Fig. 3 for the 15 eV or 16 eV plot, the calculations with N_{open} = 38 and 89 were performed at 16 eV, while those with N_{open} = 1 and 11 were undertaken at 15 eV. This was done in order to avoid being close to the energetic opening of a channel with energy near 15 eV in the expanded channel space. In order to illustrate the multichannel coupling effect, we compare the cross sections obtained according to the different channel coupling schemes, starting from the 1ch-SE approximation, where only the elastic channel is open, to the 89ch-SEP level, which is our most complete calculation having 89 open channels (the ground state plus 44 singlet states and 44 triplet states). It is clear from Figs. 3 and 4 that the main effect of multichannel coupling, particularly for scattered electron angles greater than about 20°, is to allow flux from the elastic channel to go into the discrete inelastic channels,[2] which explains the observed decrease in magnitude in the elastic DCS as more channels open up. Indeed for all the energies studied, we see a significant drop in magnitude in the elastic DCS, at middle and backward angles, as we go from the 1ch-SE results to those for our best calculation (i.e., with all 89 channels open). On the other hand, our DCS results at the 38ch-SEP and 89ch-SEP levels of approximation are very similar at all energies. This suggests that the 89ch-SEP results, at least with respect to the electronic-state inelastic channels (since there are no ionisation channels currently included in these calculations), are converged up to 50 eV.

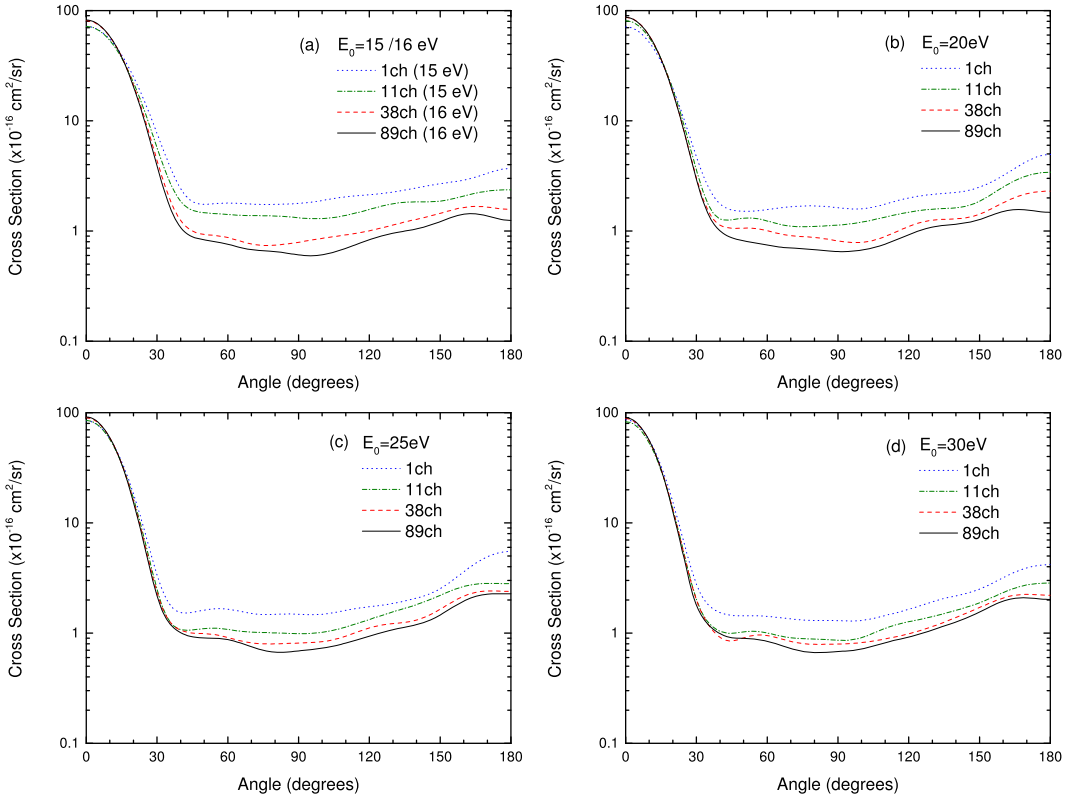

FIG. 3. Elastic scattering DCS ($\times 10^{-16}$ cm^2/sr) at (a) 15/16 eV, (b) 20 eV, (c) 25 eV, and (d) 30 eV for pBQ calculated at the SMCPP-SEP level using different channel coupling schemes (N_{open} = 1-89ch). See also the legend in the figure.

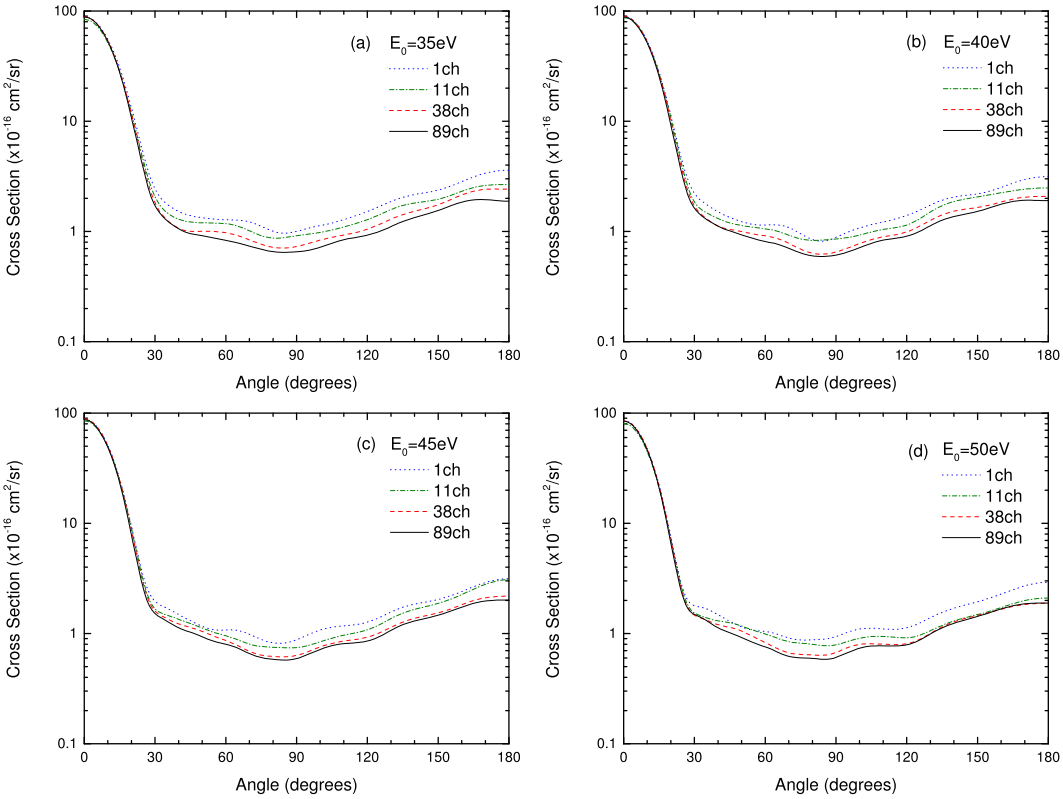

FIG. 4. Elastic scattering DCS ($\times 10^{-16}$ cm^2/sr) at (a) 35 eV, (b) 40 eV, (c) 45 eV, and (d) 50 eV for pBQ calculated at the SMCPP-SEP level using different channel coupling schemes (N_{open} = 1-89ch). See also the legend in the figure.

In Fig. 5, we plot the present SMCPP-SEP 89ch elastic DCS results, at 15/16 eV, 20 eV, 30 eV, and 40 eV incident electron energies, against our corresponding IAM-SCAR+I cross sections, for both pBQ and benzene, and also some experimental elastic DCS for benzene from the work of Cho *et al.*[95] As can be seen from Fig. 1, pBQ and benzene have similar molecular structures, in which a H-atom in the 1 and 4 positions on the benzene ring is replaced with an O-atom. In addition, both these species are non-polar and their dipole polarisabilities are similar (11.23 Å for pBQ and 9.96 Å for benzene[96]). Furthermore, in our earlier work on phenol [a compound in which a H-atom in benzene is replaced by a hydroxyl (OH) group],[42] we found very good accord between the phenol SMCPP calculation results and the elastic benzene DCS measurements[95] across the common scattered electron angular range. This was in spite of phenol being polar while benzene is non-polar. That observation was interpreted, at least in part, as reflecting that the elastic scattering dynamics in those systems are dominated by scattering from the highly polarisable ring structure which is common to both. Finally, in Fig. 5, we also see that our IAM-SCAR+I elastic DCS results, at each energy, are similar for both pBQ and benzene which therefore suggests, *a priori*, that comparing our pBQ theory results with the measured benzene results is not unreasonable. It is clear from Fig. 5 that here we also found good agreement between our SMCPP-SEP 89ch computations and the data of Cho *et al.*,[95] at 15 eV, 20 eV, 30 eV, and 40 eV, but now only for scattered electron angles less than about 60°. We believe that the difference between this latter observation in pBQ and what we found previously in phenol[42] is likely due to each of the O-atoms in pBQ (see Fig. 1) disrupting the ring bonding network. Here the doubly bonded oxygen atoms disrupt the aromatic bonding within the ring. This property significantly increases the chemical reactivity of pBQ as compared to benzene, and we believe that it plays a role in the different middle and backward angle elastic cross section data of pBQ compared to that of benzene. Particularly at the lower energies (15 and 20 eV) of this investigation, agreement between our pBQ IAM-SCAR+I and SMCPP-SEP computations is quite marginal. This is perhaps a little unsurprising as even with the SCAR and I corrections, the IAM-SCAR+I approach is not necessarily expected to be very accurate at lower electron impact energies. At 30 eV and 40 eV, their level of accord is somewhat improved, and it might even be argued (see Fig. 5) that at those energies and for $\theta \geqslant 80°$, the IAM-SCAR+I result is actually in better agreement with the benzene measurements[95] than the SMCPP-SEP results. Nonetheless, in considering Fig. 5 in its totality, it is evident to us that it is the SMCPP-SEP results that we should employ to make the normalisation of our experimental composite vibrational-excitation data.

In Tables III–V and in Fig. 6, we present our measured composite vibrational excitation cross sections for electron scattering from pBQ. In Tables III–V, we also give values of the ratios for the inelastic to elastic scattering intensities, which over all θ typically lie in the range $\sim 10^{-1}$–10^{-4}. It is therefore apparent that at the intermediate energies of this investigation, the vibrational excitation probability is significantly smaller than that for elastic scattering. This is in fact a well-known phenomenon,[94] where it is intuitively reasonable to expect that the

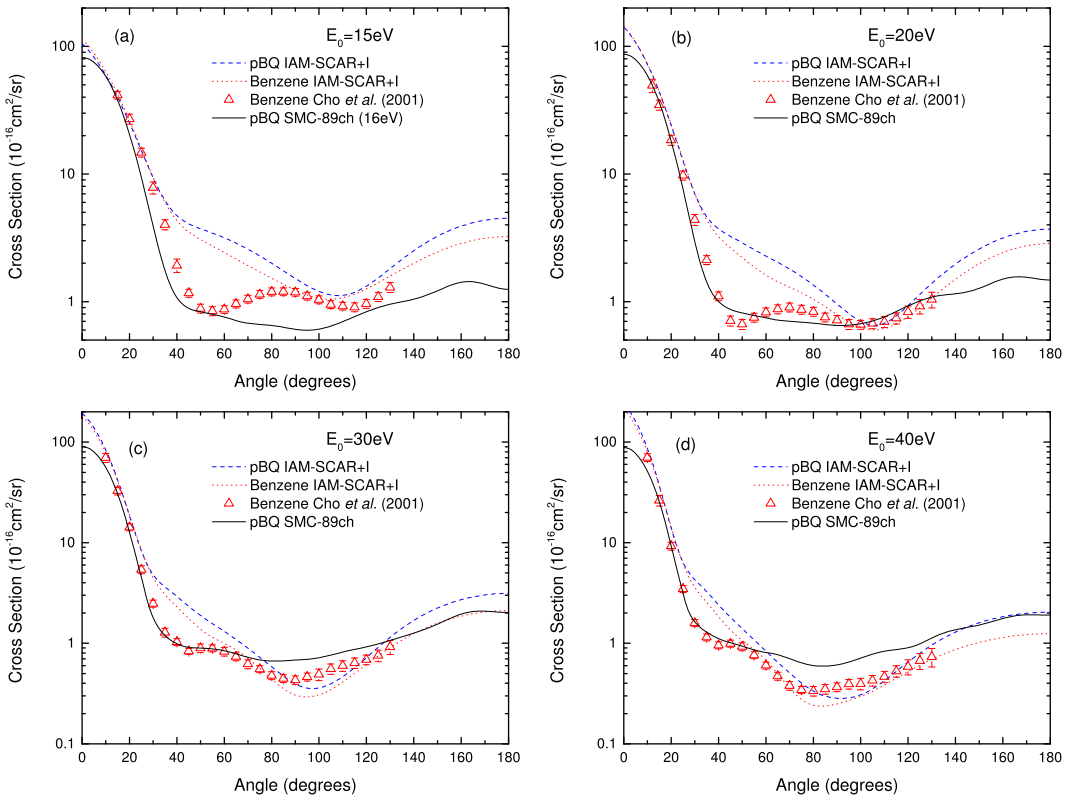

FIG. 5. Comparison of elastic scattering DCS ($\times 10^{-16}$ cm^2/sr) for pBQ and benzene at (a) 15 eV, (b) 20 eV, (c) 30 eV, and (d) 40 eV. Here we consider the experimental elastic scattering data from benzene measured by Cho *et al.*,[95] IAM-SCAR+I calculations for both benzene and pBQ, and the SMCPP-SEP 89ch calculation for pBQ. See also the legend in the figure.

relatively light incident electron will have difficulty in inducing nuclear motion of the much heavier atoms that constitute the molecule in question.[66] Indeed, vibrational excitation only leads to significant cross sections, in terms of their contribution to the total scattering cross section,[53] when the incident electrons are temporarily captured by the target species and subsequently autodetach leaving that species in one or more vibrationally excited levels. Nonetheless, just because a cross section is small at intermediate energies does not mean that we can ignore it. Do *et al.*[30] quite recently demonstrated the importance of intermediate energy vibrational-excitation cross sections in tetrahydrofuran (THF), when seeking to model the behaviour of a swarm of electrons moving through THF under the influence of an applied external electric field. Similarly, the role of intermediate energy electron-impact vibrational excitation cross sections in simulating charged-particle tracks in pyrimidine[59] was also found to be important, particularly near the end of the tracks, in achieving accurate results. We therefore expect that these same observations will also be relevant when simulating electron transport through pBQ so that the present results are potentially important to include in any pBQ cross section database that is assembled for modelling purposes.

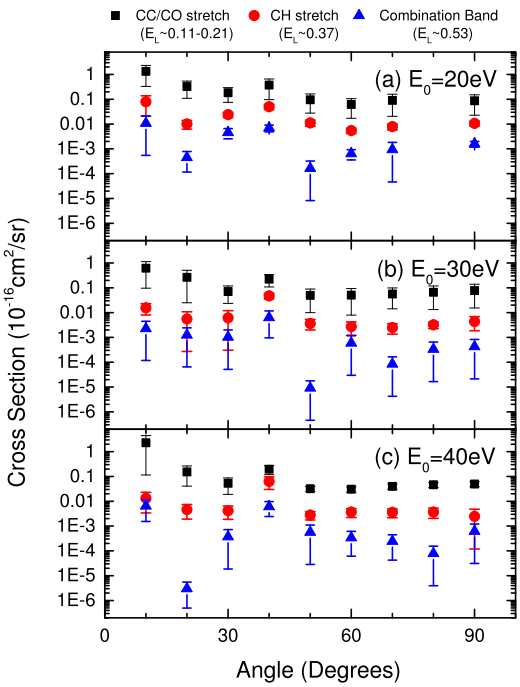

FIG. 6. Present composite vibrational (bands I, II, and III) excitation cross sections ($\times 10^{-16}$ cm^2/sr) for electron scattering from pBQ. See Table II and the legend at the top of the figure for further details.

Let us now consider Fig. 6 in more detail. Here we observe that at each energy the shapes of the pBQ composite vibrational mode DCSs, i.e., their angular distributions, for all of bands I, II, and III are typically very similar. In particular we find that, to within the uncertainties on the various cross sections, all the band I–III cross sections at 20 eV and 30 eV are largely quasi-isotropic. In addition, at 40 eV, the band II and band III angular distributions are also quasi-isotropic. The tendency for the angular distributions of composite

vibrational modes to be quasi-isotropic, at energies in the range of ~15–40 eV, has been observed by us previously in THF,[30] α-tetrahydrofurfuryl alcohol,[39] pyrimidine,[34] phenol,[43] and furfural[49] and still awaits a definitive explanation from theory. Nonetheless, if we might speculate briefly, it appears reasonable to describe vibrational excitation at intermediate energies within the adiabatic vibrational approximation (AVA),[97] which essentially assumes a fast collision in the time scale of vibrational excitations, $\hbar/\Delta E_{\nu'\leftarrow\nu}$. The AVA scattering amplitude is given by

$$f_{\nu'\leftarrow\nu}(\mathbf{k}_f, \mathbf{k}_i) \approx \left\langle \nu' \left| f(\mathbf{k}_f, \mathbf{k}_i; \mathbf{q}) \right| \nu \right\rangle, \tag{8}$$

where $\mathbf{k}_{i(f)}$ again denotes the incoming (outgoing) wave vector, $f_{\nu'\leftarrow\nu}(\mathbf{k}_f, \mathbf{k}_i)$ is the scattering amplitude for $\nu' \leftarrow \nu$ vibrational transition, and $|\nu\rangle$ is a vibrational eigenstate of the target molecule. $f(\mathbf{k}_f, \mathbf{k}_i; \mathbf{q})$ is the fixed-nuclei scattering amplitude and the semicolon (; $\mathbf{q}$) indicates the parametric dependence on the target vibrational coordinates, $\mathbf{q} = (q_1, q_2, \ldots, q_{3N-6})$.

To obtain $f_{\nu'\leftarrow\nu}(\mathbf{k}_f, \mathbf{k}_i)$, we must solve the scattering problem for a number of target geometries ($\mathbf{q}$) to allow for the numerical integration of the matrix element in Eq. (8), i.e.,

$$\left\langle \nu' \left| f(\mathbf{k}_f, \mathbf{k}_i; \mathbf{q}) \right| \nu \right\rangle = \int d\mathbf{q}\ \phi^*_{\nu'}(\mathbf{q}) f(\mathbf{k}_f, \mathbf{k}_i; \mathbf{q}) \phi_\nu(\mathbf{q}). \tag{9}$$

It is a common practice, even in resonant scattering, to assume that the angular distributions are weakly dependent on the vibrational coordinates, i.e., the scattering amplitude would have the same dependence on $\mathbf{k}_{i(f)}$ for any geometry $\mathbf{q}$. If we further assume a first-order dependence of the fixed-nuclei scattering amplitudes on $\mathbf{q}$, Eq. (9) can be recast as

$$\int d\mathbf{q}\ \phi^*_{\nu'}(\mathbf{q}) f(\mathbf{k}_f, \mathbf{k}_i; \mathbf{q}) \phi_\nu(\mathbf{q}) \approx \nabla_{\mathbf{q}} f(\mathbf{k}_f, \mathbf{k}_i; \mathbf{0}) \cdot \int d\mathbf{q}\ \phi^*_{\nu'}(\mathbf{q}) \mathbf{q} \phi_\nu(\mathbf{q}). \tag{10}$$

In the above expression, the integral over $d\mathbf{q}$ becomes trivial in the case when the target is assumed to be a system of decoupled harmonic oscillators. The gradient $\nabla_{\mathbf{q}} f(\mathbf{k}_f, \mathbf{k}_i; \mathbf{0})$, calculated at the equilibrium geometry $\mathbf{q} = 0$, would have angular dependencies essentially identical to the fixed-nuclei scattering amplitudes if the assumptions described above are valid. Restricting ourselves to the fundamental excitations of single modes ($1 \leftarrow 0$), described in the harmonic approximation, we have

$$\left\langle 1_\alpha \left| f(\mathbf{k}_f, \mathbf{k}_i; \mathbf{q}) \right| 0_\alpha \right\rangle \approx \sqrt{\frac{\hbar}{2\mu_\alpha \omega_\alpha}} \frac{\partial}{\partial q_\alpha} f(\mathbf{k}_f, \mathbf{k}_i; \mathbf{0}), \tag{11}$$

where μ_α and ω_α are the reduced mass and frequency of the αth vibrational mode, q_α. In the case of several modes undergoing fundamental excitations in a given band, the corresponding DCS will be given by

$$\frac{d\sigma^{\text{band}}}{d\Omega} \approx \sum_{\alpha \epsilon \text{band}} \frac{k_{f_\alpha}}{k_i} \left| \sqrt{\frac{\hbar}{2\mu_\alpha \omega_\alpha}} \frac{\partial}{\partial q_\alpha} f(\mathbf{k}_f, \mathbf{k}_i; \mathbf{0}) \right|^2. \tag{12}$$

The main "conclusions" from this analysis are (i) we would expect the vibrational bands to show angular dependencies similar to those of the fixed-nuclei cross sections and (ii) an improved description of the collision would consider different $\mathbf{k}_f$ wave vectors for the excitation of different modes (in view of the different excitation energies). This improvement could be achieved with the FONDA scheme of Morrison and co-workers,[98] which, in very simple terms, introduces appropriate off-shell energies in the exit channels. Thus, what Eq. (12) suggests is that the observed quasi-isotropic angular distribution behaviour, for many of the composite modes of bands I–III, is not the result of quantum interference effects but rather appears to be due to a "classical" superposition of the cross sections that make up the respective bands.

Only at 40 eV and for band I do we see an angular distribution behaviour, specifically the DCS increasing in magnitude as you go to smaller scattered electron angles, that we might interpret in terms of the target molecular properties (namely, here, its quite significant dipole polarisability[96]). In terms of the pBQ band I, band II, and band III cross section magnitudes, it is clear from Fig. 6 that typically $\text{DCS}_{\text{bandI}} \gg \text{DCS}_{\text{bandII}} \gg \text{DCS}_{\text{bandIII}}$. As bands I and II are largely composed of pBQ's fundamental normal modes, whereas band III is made up of combination bands (see Table II), this observation in regards to the DCS magnitudes is not surprising. It is well known from IR spectroscopy that the intensities of the fundamental modes of a molecule are greater than those for their overtone and combination lines. Essentially, this is the same behaviour that we are observing here for the band III DCSs relative to those for bands I and II (see Fig. 6). In the case of the magnitude of the band I DCSs being significantly larger than those for band II, given that both of these composite bands are composed of fundamental stretching and bending modes (band I only), there is in fact no contradiction. This follows as band I consists of 19 vibrational modes, while band II consists of only 4 vibrational modes (see Table II). Hence the difference between their magnitudes is we believe largely due to a density of states argument, whereby as band I incorporates about 5 times as many of the modes as band II, it follows that one might reasonably anticipate that its DCSs would be larger.

Finally, we note that there are no other experimental data or theoretical results that we can compare the current composite vibrational cross section data against. In forming a cross section database for any prospective modelling studies, it is better to be able to construct such a database from results from 2 or more independent investigations. We therefore think it would be desirable for our colleagues to also study this scattering system. Please note that we do not underestimate the difficulty for theorists in moving away from a fixed nuclei framework, in order to calculate vibrational cross sections. However this has been attempted in the past[99,100] with some success although in those cases we note that the target molecules were both homonuclear diatomics.

IV. CONCLUSIONS

We have reported on a joint theoretical and experimental study into electron scattering from 1,4-benzoquinone. Our SMCPP-SEP elastic DCS computations were performed with 89 open states, by far the largest number of open states that we have thus far incorporated into our calculations, and we believe

they are converged. We therefore employed them to normalise our measured vibrational excitation DCSs. All the calculated SMCPP-SEP intermediate energy elastic DCSs were found to be forward peaked in magnitude, entirely consistent with our IAM-SCAR+I results and with the quite significant magnitude for the molecular dipole polarisability[96] of pBQ. However while agreement between both our calculations improved as E_0 increased, we can overall only characterise the level of accord between them as being quite marginal. We believe this reflects on our SCAR with I corrections as not being totally effective in this case. While all the elastic DCSs were strongly peaked at the forward scattered electron angles, in the 20–40 eV incident electron energy range, the vast majority of our measured composite vibrational excitation (bands I–III) angular distributions were quasi-isotropic in form. The underlying reason behind this quasi-isotropy remains unclear, waiting for theory beyond the fixed nuclei approximation to help clarify.

There were, to the best of our knowledge, no other measured or calculated data in pBQ against which we could compare our results. This is a situation which we believe needs to be rectified, particularly in terms of forming a cross section database for modelling electron transport in such an important biomolecule as pBQ is. Finally, we note that the present investigation is the third[1,2] in a series from us that seeks to provide information on pBQ's structure, dynamics, and cross section. The next (fourth) paper will focus on its discrete electron impact electronic-state excitation DCSs, to be followed by a paper that details integral cross sections for the scattering processes considered here as well as the electronic-state excitation, the total ionisation, and the total cross section. Thereafter, results from an electron swarm study in pBQ, to test the self-consistency of the assembled cross section database, will be provided.

ACKNOWLEDGMENTS

This study has been partially supported by the Spanish Ministry MINECO (Project No. FIS2016-80440), COST (CM301 Action) and ITN-Marie Curie (No. ARGENT-608163) European Union programmes. M.A.P.L., M.T.do.N.V. (Grant No. 305672/2014-2), R.F.C., and M.H.F.B. all acknowledge financial support from CNPq, while F.K. (Grant No. 2015/23792-5) and M.T.do.N.V. (Grant No. 2014/10012-9) also thank FAPESP for financial support. Finally, M.J.B. (No. DP160102787) and R.D.W. acknowledge the Australian Research Council for funding.

[1]D. B. Jones, E. Ali, C. G. Ning, J. Colgan, O. Ingólfsson, D. H. Madison, and M. J. Brunger, J. Chem. Phys. **145**, 164306 (2016).
[2]D. B. Jones, P. Limão-Vieira, M. Mendes, N. C. Jones, S. V. Hoffman, R. F. da Costa, M. T. d. N. Varella, M. H. F. Bettega, F. Blanco, G. García, O. Ingólfsson, M. A. P. Lima, and M. J. Brunger, J. Chem. Phys. **146**, 184303 (2017).
[3]B. Huskinson, M. P. Marshak, C. Suh, S. Er, M. R. Gerhardt, C. J. Galvin, X. Chen, A. Aspuru-Guzik, R. G. Gordan, and M. J. Aziz, Nature **505**, 195 (2014).
[4]D. R. Choudhury, Environ. Sci. Technol. **16**, 102 (1982).
[5]T. Itoh, Chem. Rev. **95**, 2351 (1995).
[6]B. Ómarsson and O. Ingólfsson, Phys. Chem. Chem. Phys. **15**, 16758 (2013).
[7]D. Dougherty and S. P. McGlynn, J. Am. Chem. Soc. **99**, 3234 (1977).
[8]J. F. Stanton, K. W. Sattelmeyer, J. Gauss, M. Allan, T. Skalicky, and T. Bally, J. Chem. Phys. **115**, 1 (2001).
[9]C. R. Brundle, M. B. Robin, and N. H. Kuebler, J. Am. Chem. Soc. **94**, 1966 (1972).
[10]L. Åsbrink, G. Bieri, C. Fridh, E. Lindholm, and D. P. Chong, Chem. Phys. **43**, 189 (1979).
[11]N. Kishimoto, K. Okamura, and K. Ohno, J. Chem. Phys. **120**, 11062 (2004).
[12]K. Piech, T. Bally, T. Ichino, and J. Stanton, Phys. Chem. Chem. Phys. **16**, 2011 (2014).
[13]J. M. Hollas, Spectrochim. Acta **20**, 1563 (1964).
[14]N. Ohta, I. Yamazaki, M. Sanekata, I. Suzuka, and O. Sekiguchi, J. Phys. Chem. **97**, 7857 (1993).
[15]G. Ter Horst and J. Kommandeur, Chem. Phys. **44**, 287 (1979).
[16]A. Sadô, Bull. Chem. Soc. Jpn. **35**, 1520 (1962).
[17]H. P. Trommsdorff, J. Chem. Phys. **56**, 5358 (1972).
[18]H. P. Trommsdorff and J. Kahane-Paillous, Spectrochim. Acta **23**, 1661 (1967).
[19]P. Brint, J.-P. Connerade, P. Tsekeris, A. Bolovinos, and A. Baig, J. Chem. Soc., Faraday Trans. 2 **82**, 367 (1986).
[20]L. G. Christophorou, J. G. Carter, and A. A. Christodoulides, Chem. Phys. Lett. **3**, 237 (1969).
[21]P. M. Collins, L. G. Christophorou, E. L. Chaney, and J. G. Carter, Chem. Phys. Lett. **4**, 646 (1970).
[22]C. D. Cooper, W. T. Naff, and R. N. Compton, J. Chem. Phys. **63**, 2752 (1975).
[23]M. Allan, Chem. Phys. **84**, 311 (1984).
[24]M. Allan, Chem. Phys. **81**, 235 (1983).
[25]A. Loupas and J. D. Gorfinkiel, Phys. Chem. Chem. Phys. **19**, 18252 (2017).
[26]P. A. Thorn, M. J. Brunger, P. J. O. Teubner, N. Diakomichalis, T. Maddern, M. A. Bolorizadeh, W. R. Newell, H. Kato, M. Hoshino, H. Tanaka, H. Cho, and Y.-K. Kim, J. Chem. Phys. **126**, 064306 (2007).
[27]P. A. Thorn, M. J. Brunger, H. Kato, M. Hoshino, and H. Tanaka, J. Phys. B: At., Mol. Opt. Phys. **40**, 697 (2007).
[28]T. P. T. Do, M. Leung, M. Fuss, G. Garcia, F. Blanco, K. Ratnavelu, and M. J. Brunger, J. Chem. Phys. **134**, 144302 (2011).
[29]M. C. Fuss, A. G. Sanz, F. Blanco, P. Limão-Vieira, M. J. Brunger, and G. García, Eur. Phys. J. D **68**, 161 (2014).
[30]T. P. T. Do, H. V. Duque, M. C. A. Lopes, D. Konovalov, R. D. White, M. J. Brunger, and D. B. Jones, J. Chem. Phys. **142**, 124306 (2015).
[31]M. C. Fuss, A. G. Sanz, F. Blanco, J. C. Oller, P. Limão-Vieira, M. J. Brunger, and G. García, Phys. Rev. A **88**, 042702 (2013).
[32]P. Palihawadana, J. Sullivan, M. Brunger, C. Winstead, V. McKoy, G. García, F. Blanco, and S. Buckman, Phys. Rev. A **84**, 062702 (2011).
[33]Z. Mašín, J. D. Gorfinkiel, D. B. Jones, S. M. Bellm, and M. J. Brunger, J. Chem. Phys. **136**, 144310 (2012).
[34]D. B. Jones, L. Ellis-Gibbings, G. García, K. L. Nixon, M. C. A. Lopes, and M. J. Brunger, J. Chem. Phys. **143**, 094304 (2015).
[35]D. B. Jones, S. M. Bellm, P. Limão-Vieira, and M. J. Brunger, Chem. Phys. Lett. **535**, 30 (2012).
[36]D. B. Jones, S. M. Bellm, F. Blanco, M. Fuss, G. García, P. Limão-Vieira, and M. J. Brunger, J. Chem. Phys. **137**, 074304 (2012).
[37]P. Limão-Vieira, D. Duflot, M.-J. Hubin-Franskin, J. Delwiche, S. V. Hoffmann, L. Chiari, D. B. Jones, M. J. Brunger, and M. C. A. Lopes, J. Phys. Chem. A **118**, 6425 (2014).
[38]H. V. Duque, L. Chiari, D. B. Jones, P. A. Thorn, Z. Pettifer, G. B. da Silva, P. Limão-Vieira, D. Duflot, M.-J. Hubin-Franskin, J. Delwiche, F. Blanco, G. García, M. C. A. Lopes, K. Ratnavelu, R. D. White, and M. J. Brunger, Chem. Phys. Lett. **608**, 161 (2014).
[39]H. V. Duque, L. Chiari, D. B. Jones, Z. Pettifer, G. B. da Silva, P. Limão-Vieira, F. Blanco, G. García, R. D. White, M. C. A. Lopes, and M. J. Brunger, J. Chem. Phys. **140**, 214306 (2014).
[40]L. Chiari, H. V. Duque, D. B. Jones, P. A. Thorn, Z. Pettifer, G. B. da Silva, P. Limão-Vieira, D. Duflot, M.-J. Hubin-Franskin, J. Delwiche, F. Blanco, G. García, M. C. A. Lopes, K. Ratnavelu, R. D. White, and M. J. Brunger, J. Chem. Phys. **141**, 024301 (2014).
[41]P. Limão-Vieira, D. Duflot, F. Ferreira da Silva, E. Lange, N. C. Jones, S. V. Hoffmann, M. A. Śmialek, D. B. Jones, and M. J. Brunger, J. Chem. Phys. **145**, 034302 (2016).
[42]R. F. da Costa, E. M. de Oliveira, M. H. F. Bettega, M. T. d. N. Varella, D. B. Jones, M. J. Brunger, F. Blanco, R. Colmenares, P. Limão-Vieira, G. García, and M. A. P. Lima, J. Chem. Phys. **142**, 104304 (2015).

[43]R. F. C. Neves, D. B. Jones, M. C. A. Lopes, K. L. Nixon, E. M. de Oliveira, R. F. da Costa, M. T. d. N. Varella, M. H. F. Bettega, M. A. P. Lima, G. B. da Silva, and M. J. Brunger, J. Chem. Phys. **142**, 194302 (2015).
[44]R. F. C. Neves, D. B. Jones, M. C. A. Lopes, F. Blanco, G. García, K. Ratnavelu, and M. J. Brunger, J. Chem. Phys. **142**, 194305 (2015).
[45]R. F. C. Neves, D. B. Jones, M. C. A. Lopes, K. L. Nixon, G. B. da Silva, H. V. Duque, E. M. de Oliveira, R. F. da Costa, M. T. d. N. Varella, M. H. F. Bettega, M. A. P. Lima, K. Ratnavelu, G. García, and M. J. Brunger, J. Chem. Phys. **142**, 104305 (2015).
[46]D. B. Jones, G. B. da Silva, R. F. C. Neves, H. V. Duque, L. Chiari, E. M. de Oliveira, M. C. A. Lopes, R. F. da Costa, M. T. d. N. Varella, M. H. F. Bettega, M. A. P. Lima, and M. J. Brunger, J. Chem. Phys. **141**, 074314 (2014).
[47]F. Ferreira da Silva, E. Lange, P. Limão-Vieira, N. C. Jones, S. V. Hoffmann, M.-J. Hubin-Franskin, J. Delwiche, M. J. Brunger, R. F. C. Neves, M. C. A. Lopes, E. M. de Oliveria, R. F. da Costa, M. T. d. N. Varella, M. H. F. Bettega, F. Blanco, G. García, M. A. P. Lima, and D. B. Jones, J. Chem. Phys. **143**, 144308 (2015).
[48]R. F. da Costa, M. T. d. N. Varella, M. H. F. Bettega, R. F. C. Neves, M. C. A. Lopes, F. Blanco, G. García, D. B. Jones, M. J. Brunger, and M. A. P. Lima, J. Chem. Phys. **144**, 124310 (2016).
[49]D. B. Jones, R. F. C. Neves, M. C. A. Lopes, R. F. da Costa, M. T. d. N. Varella, M. H. F. Bettega, M. A. P. Lima, G. García, F. Blanco, and M. J. Brunger, J. Chem. Phys. **143**, 224304 (2015).
[50]D. B. Jones, R. F. C. Neves, M. C. A. Lopes, R. F. da Costa, M. T. d. N. Varella, M. H. F. Bettega, M. A. P. Lima, G. García, P. Limão-Vieira, and M. J. Brunger, J. Chem. Phys. **144**, 124309 (2016).
[51]D. B. Jones, R. F. da Costa, M. T. d. N. Varella, M. H. F. Bettega, M. A. P. Lima, F. Blanco, G. García, and M. J. Brunger, J. Chem. Phys. **144**, 144303 (2016).
[52]A. Traoré Dubuis, A. Verkhovtsev, L. Ellis-Gibbings, K. Krupa, F. Blanco, D. B. Jones, M. J. Brunger, and G. García, J. Chem. Phys. **147**, 054301 (2017).
[53]M. J. Brunger, Int. Rev. Phys. Chem. **36**, 333 (2017).
[54]J. D. Gorfinkiel and S. Ptasinska, J. Phys. B: At., Mol. Opt. Phys. **50**, 182001 (2017).
[55]L. C. Pitchford, L. L. Alves, K. Bartschat, S. F. Biagi, M.-C. Bordage, I. Bray, C. E. Brion, M. J. Brunger, L. Campbell *et al.*, Plasma Processes Polym. **14**, 1600098 (2017).
[56]A. G. Sanz, M. C. Fuss, A. Muñoz, F. Blanco, P. Limão-Vieira, M. J. Brunger, S. J. Buckman, and G. García, Int. J. Radiat. Biol. **88**, 71 (2012).
[57]M. C. Fuss, L. Ellis-Gibbings, D. B. Jones, M. J. Brunger, F. Blanco, A. Muñoz, P. Limão-Vieira, and G. García, J. Appl. Phys. **117**, 214701 (2015).
[58]M. J. Brunger, K. Ratnavelu, S. J. Buckman, D. B. Jones, A. Muñoz, F. Blanco, and G. García, Eur. Phys. J. D **70**, 46 (2016).
[59]A. I. Lozano, K. Krupa, F. Ferreira da Silva, P. Limão-Vieira, F. Blanco, A. Munõz, D. B. Jones, M. J. Brunger, and G. García, Eur. Phys. J. D **71**, 226 (2017).
[60]K. F. Ness, R. E. Robson, M. J. Brunger, and R. D. White, J. Chem. Phys. **136**, 024318 (2012).
[61]N. A. Garland, M. J. Brunger, G. Garcia, J. de Urquijo, and R. D. White, Phys. Rev. A **88**, 062712 (2013).
[62]R. D. White, M. J. Brunger, N. A. Garland, R. E. Robson, K. F. Ness, G. Garcia, J. de Urquijo, S. Dujko, and Z. L. Petrović, Eur. Phys. J. D **68**, 125 (2014).
[63]J. de Urquijo, E. Basurto, A. M. Juárez, K. F. Ness, R. E. Robson, M. J. Brunger, and R. D. White, J. Chem. Phys. **141**, 014308 (2014).
[64]H. V. Duque, T. P. T. Do, M. C. A. Lopes, D. A. Konovalov, R. D. White, M. J. Brunger, and D. B. Jones, J. Chem. Phys. **142**, 124307 (2015).
[65]M. J. E. Casey, J. de Urquijo, L. N. Serkovic Loli, D. G. Cocks, G. J. Boyle, D. B. Jones, M. J. Brunger, and R. D. White, J. Chem. Phys. **147**, 195103 (2017).
[66]H. Tanaka, M. J. Brunger, L. Campbell, H. Kato, M. Hoshino, and A. R. P. Rau, Rev. Mod. Phys. **88**, 025004 (2016).
[67]K. Takatsuka and V. McKoy, Phys. Rev. A **24**, 2473 (1981); **30**, 1734 (1984).
[68]J. S. dos Santos, R. F. da Costa, and M. T. d. N. Varella, J. Chem. Phys. **136**, 084307 (2012).
[69]M. H. F. Bettega, L. G. Ferreira, and M. A. P. Lima, Phys. Rev. A **47**, 1111 (1993).
[70]R. F. da Costa, F. J. da Paixão, and M. A. P. Lima, J. Phys. B **37**, L129 (2004).
[71]R. F. da Costa, M. T. d. N. Varella, M. H. F. Bettega, and M. A. P. Lima, Eur. Phys. J. D **69**, 159 (2015).
[72]M. A. P. Lima, T. L. Gibson, K. Takatsuka, and V. McKoy, Phys. Rev. A **30**, 1741 (1984).
[73]F. Blanco, J. Rosada, A. Illana, and G. García, Phys. Lett. A **374**, 4420 (2010).
[74]F. Blanco, L. Ellis-Gibbings, and G. García, Chem. Phys. Lett. **645**, 71 (2016).
[75]F. Blanco and G. García, J. Phys. B: At., Mol. Opt. Phys. **42**, 145203 (2009).
[76]R. D. Cowan, *The Theory of Atomic Structure and Spectra* (University of California Press, London, 1981).
[77]M. E. Riley and D. G. Truhlar, J. Chem. Phys. **63**, 2182 (1975).
[78]X. Zhang, J. Sun, and Y. Liu, J. Phys. B: At., Mol. Opt. Phys. **25**, 1893 (1992).
[79]G. Staszewska, D. W. Schwenke, D. Thirumalai, and D. G. Truhlar, Phys. Rev. A **28**, 2740 (1983).
[80]F. Blanco and G. García, Phys. Lett. A **295**, 178 (2002).
[81]F. Blanco and G. García, Phys. Rev. A **67**, 022701 (2003).
[82]O. Zatsarinny, K. Bartschat, G. Garcia, F. Blanco, L. R. Hargreaves, D. B. Jones, R. Murrie, J. R. Brunton, M. J. Brunger, M. Hoshino, and S. J. Buckman, Phys. Rev. A **83**, 042702 (2011).
[83]Y. Jiang, J. Sun, and L. Wan, Phys. Rev. A **52**, 398 (1995).
[84]F. Blanco and G. García, Phys. Lett. A **317**, 458 (2003); **330**, 230 (2004).
[85]M. Fuss, A. Muñoz, J. C. Oller, F. Blanco, D. Almeida, P. Limão-Vieira, T. P. D. Do, M. J. Brunger, and G. García, Phys. Rev. A **80**, 052709 (2009).
[86]L. R. Hargreaves, J. R. Brunton, A. Prajapati, M. Hoshino, F. Blanco, G. Garcia, S. J. Buckman, and M. J. Brunger, J. Phys. B: At., Mol. Opt. Phys. **44**, 045207 (2011).
[87]H. Kato, A. Suga, M. Hoshino, F. Blanco, G. García, P. Limão-Vieira, M. J. Brunger, and H. Tanaka, J. Chem. Phys. **136**, 134313 (2012).
[88]M. J. Brunger and P. J. O. Teubner, Phys. Rev. A **41**, 1413 (1990).
[89]T. M. Maddern, V. Jamier, J. R. Brunton, M. J. Brunger, C. Papamicaël, S. V. Smith, and S. J. Buckman, Int. J. Mass Spectrom. **409**, 73 (2016).
[90]J. Weber, K. Malsch, and G. Hohlneicher, Chem. Phys. **264**, 275 (2001).
[91]M. J. Frisch *et al.*, GAUSSIAN 09, Revision B.01, Gaussian, Inc., 2010.
[92]L. Campbell, M. J. Brunger, P. J. O. Teubner, B. Mojarrabi, and D. C. Cartwright, Aust. J. Phys. **50**, 525 (1997).
[93]M. Allan, J. Phys. B: At., Mol. Opt. Phys. **38**, 3655 (2005).
[94]M. J. Brunger and S. J. Buckman, Phys. Rep. **357**, 215 (2002).
[95]H. Cho, R. J. Gulley, K. Sunohara, M. Kitajima, L. J. Uhlmann, H. Tanaka, and S. J. Buckman, J. Phys. B: At., Mol. Opt. Phys. **34**, 1019 (2001).
[96]M. Gussoni, M. Rui, and G. Zerbi, J. Mol. Struct. **447**, 163 (1998).
[97]D. M. Chase, Phys. Rev. **104**, 838 (1956).
[98]M. A. Morrison, M. Abdolsalami, and B. K. Elza, Phys. Rev. A **43**, 3440 (1991).
[99]C. J. Noble, K. Higgins, G. Wöste, P. Duddy, P. G. Burke, P. J. O. Teubner, A. G. Middleton, and M. J. Brunger, Phys. Rev. Lett. **76**, 3534 (1996).
[100]S. J. Buckman, M. J. Brunger, D. S. Newman, G. Snitchler, S. Alston, D. W. Norcross, M. A. Morrison, B. C. Saha, G. Danby, and W. K. Trail, Phys. Rev. Lett. **65**, 3253 (1990).